Performance Evaluation of UWB Signal Transmission over Optical Fiber

Shilong Pan, *Member, IEEE,* and Jianping Yao, *Senior Memeber, IEEE*

***Abstract*—UWB over fiber (UWBoF) technique has been proposed to increase the area of coverage for UWB communication systems. In this paper, the transmission performance of impulse UWB signals over optical fiber is analyzed. Three types of UWB signals generated based on three different techniques are considered. Since optical signals with different optical spectra would have different tolerances to fiber dispersion, the transmission performance of the three types of UWB signals is studied. First, the impact of fiber chromatic dispersion on UWB waveforms and their spectra is evaluated. Then, the transmission performance of data-modulated UWB signals in an optical fiber is investigated, with a general model to analyze the signal power spectral density (PSD) being developed. The PSD of an UWB signal with on-off keying (OOK), bi-phase modulation (BPM) and pulse position modulation (PPM) schemes is calculated. Evolution of the PSD as a function of transmission distance is then performed. The suitability of the three types of UWB signals for UWBoF applications is also evaluated. The study provides a guideline for the design and development of a practical UWBoF system.**

***Index Terms*—Ultrawideband (UWB), power spectral density (PSD), optical fiber, external modulation, photonic microwave filter, radio over fiber, microwave photonics.**

I. Introduction

ULTRAWIDEBAND (UWB) is considered a promising solution for future high data-rate and short-range wireless communication systems, to meet an ever growing demand for wide bandwidth and high speed [1]–[4]. The key feature of an UWB system is the ability to spread a signal over a sufficiently wide bandwidth to ensure a low power density with negligible interferences with existing wireless systems. In 2002, the U.S. Federal Communications Commission (FCC) approved unlicensed use of a spectral band from 3.1 to 10.6 GHz with a transmitted power spectral density (PSD) of less than -41.3 dBm/MHz for indoor wireless communications. Due to the low power density of the transmitted signal, the communication distance of an UWB system is limited to a few meters to tens of meters. To increase the area of coverage, a new technique to distribute UWB signals over optical fiber, or UWB over fiber (UWBoF), is proposed [5]–[17]. In an UWBoF system, UWB signals are generated in the central office (CO) and distributed to the access points (APs) via optical fiber [5].

For UWB communications, the primary task is to generate UWB signals that have a PSD meeting the FCC spectral mask. An UWB signal can be generated in the electrical domain and then converted to the optical domain based on direct modulation of a laser source [17]. To avoid using extra electrical to optical conversion, UWB signals can also be generated directly in the optical domain. For example, an UWB signal can be generated in the optical domain based on spectral shaping and dispersion-induced frequency-to-time mapping [18], [19]. However, these techniques suffer severely from the frequency chirp and therefore the UWB pulses are easily distorted due to the chromatic dispersion (CD) of an optical fiber. To reduce the distortions, the transmission distance should be short [19] or dispersion compensation has to be employed [11], which may increase the system complexity and the cost. To overcome the problem, techniques to generate UWB signals with zero or small chirp have been recently proposed [6], [7], [20]–[31]. These techniques include the employment of external intensity modulation (IM) based on a Mach-Zehnder modulator (MZM) [6], [7], optical phase modulation (PM) and phase modulation-to-intensity modulation (PM-to-IM) conversion [21]–[23], and the employment of a two- or three-tap photonic microwave delay-line filter with one negative tap coefficient [24]–[30]. Although these techniques have been already reported in literature, the study on the fiber transmission performance of the UWB pulses generated based on these techniques has not been reported.

For an impulse UWBoF system, the information must be encoded using pulse modulation schemes, such as on-off keying (OOK), bi-phase modulation (BPM, also known as pulse-polarity modulation), pulse-position modulation (PPM) and pulse-shape modulation (PSM). UWB signals with different modulation schemes would have different PSD. Generally, the PSD of an UWB signal consists of continuous and discrete components. The discrete components contribute more to the PSD, therefore they would cause more interferences to narrowband wireless systems [32]. A technique called time hopping (TH) is thus proposed to reduce the discrete lines in the PSD. Because UWB signals should co-exist with other narrowband wireless systems operating in the same frequency range with negligible mutual interferences, the PSD of an UWB signal is very important for the design and deployment of a practical UWB system. In the past, the PSD of electrical UWB signals with and without TH were computed [32]–[38]. However, no investigation about the PSD of UWB signals in an UWBoF system has been reported.

In this paper, we theoretically study the transmission performance of an UWB signal propagating in an optical fiber. Since a Gaussian monocycle is the simplest pulse shape among the many suggested UWB waveforms [3], our study would be

Manuscript received 15 August 2009; revised 20 January 2010. This work was supported by the Natural Sciences and Engineering Research Council of Canada (NSERC).

The authors are with the Microwave Photonics Research Laboratory, School of Information Technology and Engineering, University of Ottawa, Ottawa, ON K1N 6N5, Canada (e-mail: jpyao@site.uOttawa.ca).

Digital Object Identifier 10.1109/JSAC.2010.100813.

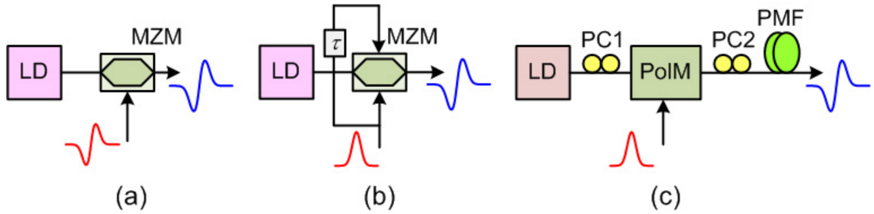

Fig. 1. Configurations of three typical techniques for generation of optical UWB monocycle pulses. (a) Generation of DSB-UWB monocycles using a MZM; (b) Generation of QSSB-UWB monocycles using a dual-drive MZM; (c) Generation of GUWB monocycles using a photonic microwave delay-line filter. LD: laser diode, MZM: Mach-Zehnder modulator, PC: polarization controller, PolM: polarization modulator, PMF: polarization maintaining fiber.

performed based on Gaussian monocycle pulses. The results can be extended to other UWB waveforms, such as Gaussian doublet, Gaussian triplet, and other more complicated waveforms.

The paper is organized as follows. In Section II, we analytically study the optical spectral properties of UWB monocycle pulses. Three types of UWB signals generated based on three different techniques are considered. The first technique to generate an UWB signal is to use external modulation based on a MZM. In this case, the modulation signal is an electrical UWB signal. The UWB signal generated based on this technique is in fact a double-sideband modulated signal, which will be called double-sideband UWB (DSB-USB). The second technique to generate an UWB signal is to use a dual-port MZM. The operation is similar but not exactly equal to single-sideband modulation. Therefore, the generated UWB signal is called quasi single-sideband UWB (QSSB-UWB). In the third technique, an UWB signal is generated using a two- or three-tap photonic microwave filter with one negative tap. The operation can be considered as a first- or second-order difference. Since an UWB monocycle is generated by subtracting two time-delayed Gaussian pulses, the UWB signal generated based on this technique is called Gaussian UWB (GUWB). A detailed discussion on the generation of the UWB signals based on the three techniques is presented in this section as well. In Section III, the evolution of the waveforms and spectra of UWB monocycle pulses as a function of transmission distance in an optical fiber is analyzed. In Section IV, a general model to analyze the PSD of an UWB signal is developed, which is used to investigate the transmission performance of data-modulated UWB signals. The impact of fiber dispersion on the PSD of an UWB signal with different modulation schemes is investigated. The influence of TH on the transmission performance is also discussed in this section. A conclusion is drawn in Section IV.

II. Optical Spectra of Gaussian Monocycles

For an UWBoF system, we assume that the transmission distance is always less than 40 km. Due to the wide bandwidth and high data rate of an UWB signal, fiber dispersion will be the major factor that would affect the transmission performance. It is known that an optical signal with a narrower bandwidth would have higher tolerance to fiber dispersion. For an UWB signal, a narrower spectral width would make it more robust to fiber dispersion. In this section, the optical spectral properties of three types of UWB signals generated by three different techniques are analytically studied.

A. DSB-UWB Monocycle Pulse

It is known that the employment of external modulation using a MZM biased at the quadrature transmission point would perform double-sideband modulation, with the generated optical signal having an optical carrier and two sidebands. If the drive signal is an electrical Gaussian monocycle, the generated optical signal would have an optical spectrum consisting of an optical carrier and two sidebands with a shape identical to the spectrum of the monocycle [6], [7].

Fig. 1(a) shows a schematic for the generation of a DSB Gaussian monocycle. The system consists of a laser diode (LD) and a MZM which is driven by an electrical Gaussian monocycle. Mathematically, if an optical carrier with an angular frequency of ω_c is injected into the MZM, the optical field at the output of the MZM can be expressed as

$$E(t) = \exp(j\omega_c t)\left\{\exp\left[j\frac{\kappa}{2}w(t) \pm j\frac{\pi}{2}\right] + \exp\left[-j\frac{\kappa}{2}w(t)\right]\right\} \quad (1)$$

where κ is the phase modulation index, and $w(t)$ is the electrical Gaussian monocycle. Since the Gaussian monocycle is the first-order derivative of a Gaussian pulse, its normalized expression is given by

$$w(t) = -\frac{t\exp(1/2)}{T_0}\exp\left(-\frac{t^2}{2T_0^2}\right) \quad (2)$$

where T_0 is the half-width (at $1/e$-intensity point) of the Gaussian pulse. In practice, it is customary to use the full width at half maximum (FWHM) in place of T_0. The two are related by

$$T_{\mathrm{FWHM}} = 2\sqrt{\ln 2}T_0 \approx 1.665T_0 \quad (3)$$

The $\pm$ in (1) corresponds to two opposite polarities. To derive (1), we assume that the MZM has zero chirp.

When the signal expressed by (1) is sent to a photodetector (PD) for square-law detection, the photocurrent at the output of the PD is given by

$$I(t) \propto 1 \mp \sin[\kappa w(t)] \approx 1 \mp \kappa w(t) \quad (4)$$

In writing (4), small signal modulation condition ($\kappa \leq \pi/6$) is assumed.

Converting (1) to the frequency domain, we have

$$\tilde{E}(\omega) = (1 \pm j)\left[2\pi\delta(\omega-\omega_c) \mp \frac{\kappa}{2}\tilde{W}(\omega-\omega_c)\right] \quad (5)$$

where $\tilde{W}(\omega) = \tilde{\mathcal{F}}\{w(t)\}$ is the Fourier transform of the input Gaussian monocycle. Accordingly, the optical spectrum of the generated optical Gaussian monocycle can be written as

$$\tilde{P}(\omega) = \left|\tilde{E}(\omega)\right|^2 \approx 8\pi^2\delta(\omega-\omega_c) + \frac{\kappa^2}{2}\tilde{W}^2(\omega-\omega_c) \quad (6)$$

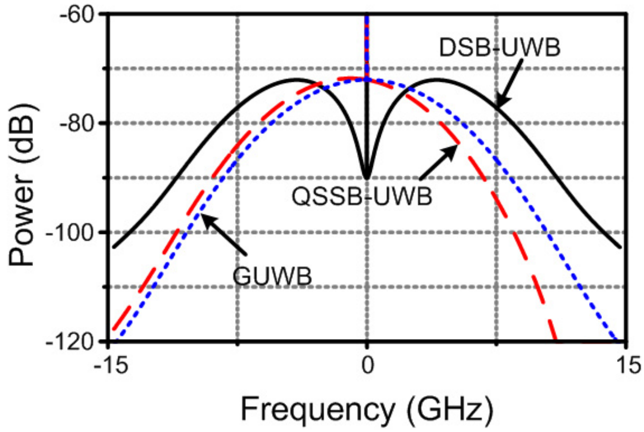

Fig. 2. Simulated optical spectra of the optical DSB-UWB (solid line), QSSB-UWB (dashed line) and GUWB (dotted line) monocycle pulses.

Since $\tilde{W}(\omega)$ has two sidebands, the optical spectrum of the generated pulse consists of an optical carrier and two sidebands. The pulse is thus called DSB-UWB monocycle.

B. QSSB-UWB Monocycle Pulse

Fig. 1(b) shows another scheme for the generation of a Gaussian monocycle [20]. A light wave from an LD is sent to a dual-drive MZM. The modulator is biased at the quadrature transmission point. A Gaussian pulse train is split into two portions and then applied to the MZM via the two RF ports. A time delay difference of τ between the two signals is introduced by an electrical delay line. The optical field at the output of the MZM can be expressed as

$$E(t) = \exp(j\omega_c t)\left\{\exp\left[j\frac{\kappa}{2}u(t) \pm j\frac{\pi}{2}\right] + \exp\left[j\frac{\kappa}{2}u(t-\tau)\right]\right\} \quad (7)$$

where $u(t)$ is a normalized Gaussian pulse which is given by

$$u(t) = \exp\left(-\frac{t^2}{2T_0^2}\right) \quad (8)$$

For small-signal modulation (i.e. $\kappa \leq \pi/6$), we have $\exp[j\kappa u(t)/2] = 1 + j\kappa u(t)/2$, then (7) is approximated

$$E(t) \approx \exp(j\omega_c t)\left\{(1 \pm j) + \frac{\kappa}{2}[ju(t-\tau) \mp u(t)]\right\} \quad (9)$$

If the signal with an expression of (9) is sent to a PD for square-law detection, we have the photocurrent at the output of the PD,

$$I(t) \propto |E_0(t)|^2 \approx 2 \pm \kappa[u(t-\tau) - u(t)] \quad (10)$$

As can be seen the AC term of the output current is proportional to the first-order difference of the input Gaussian pulse. If τ is sufficiently small, the first-order difference can be approximated as the first-order derivative, therefore the entire system is equivalent to a first-order differentiator. A Gaussian monocycle is thus generated. Since the phase of $E(t)$ varies with t, the optical QSSB-UWB pulse is chirped.

Converting (9) to the frequency domain, we have

$$\tilde{E}(\omega) = 2\pi(1 \pm j)\delta(\omega-\omega_c) + \frac{\kappa}{2}\left[je^{-j(\omega-\omega_c)\tau} \mp 1\right]\tilde{U}(\omega-\omega_c) \quad (11)$$

where $\tilde{U}(\omega) = \tilde{\mathcal{F}}\{u(t)\}$ is the Fourier transform of the input Gaussian monocycle. Correspondingly, the optical spectrum can be written as

$$\tilde{P}(\omega) = \left|\tilde{E}(\omega)\right|^2 \approx 8\pi^2\delta(\omega-\omega_c) + \frac{\kappa^2}{2}[1 \pm \sin(\omega-\omega_c)\tau]\,\tilde{U}^2(\omega-\omega_c) \quad (12)$$

As can be seen from (12), the optical spectrum is asymmetric, which consists of an optical carrier and a Gaussian lobe filtered by a system having a sine-based asymmetry transfer function. The profile would be similar to the optical spectrum of a single sideband plus carrier (SSB+C) signal. The pulse is thus named as QSSB-UWB monocycle.

It should be noted that an asymmetric optical spectrum can also be produced by the UWB monocycle generation technique in [21]–[23], where an UWB monocycle is generated based on PM and PM-to-IM conversion. Specifically, a continuous-wave light is first phase modulated by an electrical Gaussian pulse and then filtered by a fiber Bragg grating (FBG) or an asymmetric Mach-Zehnder interferometer (AMZI). The FBG or AMZI introduces an imbalance loss to the left and right sides of the optical carrier, which performs the PM-IM conversion leading to the generation of a Gaussian monocycle.

C. GUWB Monocycle Pulse

It is known that the first-order difference can be implemented by a two-tap photonic microwave delay-line filter having a positive and a negative taps, and the operation can be approximated as a first-order differentiation if the time delay is sufficiently small. Therefore, a Gaussian monocycle can be produced if the input electrical signal is a Gaussian pulse [5], [13], [24]–[30]. When designing a photonic microwave delay-line filter, to avoid optical interference, incoherent detection is employed which can be achieved by using two independent wavelengths corresponding to the two taps or a single wavelength but with two orthogonally polarized states. Since the detection is incoherent, the optical spectrum of the generated pulse is simply an addition of the optical spectra of the time-delayed signals. When the input signal is an electrical Gaussian pulse, the optical spectra of the time-delayed signals consist of an optical carrier and a Gaussian lobe. As a result, the generated Gaussian monocycle has one or two optical carriers and one or two Gaussian lobes Fig. 1(c) shows a two-tap photonic microwave delay-line filter with two coefficients (1, -1) [25], which consists of a LD, a polarization modulator (PolM), two polarization controllers (PCs) and a section of polarization-maintaining fiber (PMF). A light wave from the LD is fiber coupled to the PolM through a PC (PC1) which is driven by a Gaussian pulse train. The PolM is a special phase modulator that can support both TE and TM modes with, however, opposite phase modulation indices. When a linearly polarized incident light is oriented at an angle of 45° to one principal axis of the PolM, complementary phase modulated signals are generated along the two principal axes. The normalized optical fields at the output of the PolM along the two principal axes can be expressed as

$$\begin{bmatrix} E_x(t) \\ E_y(t) \end{bmatrix} = \exp\left(j\omega_c t\right) \begin{bmatrix} \exp\left[j\kappa u(t)/2\right] \\ \exp\left[-j\kappa u(t)/2\right] \end{bmatrix} \tag{13}$$

The optical signals are then sent to a PMF-based delay line through a second PC (PC2), which is used to align the principal axes of the PolM to have an angle of 45° with the principal axes of the PMF. The optical fields at the output of the PMF along the two principal axes of the PMF can be written as

$$\begin{bmatrix} E'_x(t) \\ E'_y(t) \end{bmatrix} = \frac{\sqrt{2}\exp\left(j\omega_c t\right)}{2} \times \begin{bmatrix} \exp\left[j\kappa u(t)/2\right] + \exp\left[-j\kappa u(t)/2 - j\phi_0\right] \\ e^{j\omega_c \tau}\left\{\exp\left[j\kappa u(t-\tau)/2\right] - \exp\left[-j\kappa u(t-\tau)/2 - j\phi_0\right]\right\} \end{bmatrix} \tag{14}$$

where ϕ_0 is a static phase shift induced by PC2 and τ is the differential group delay (DGD) of the PMF. If the signal from the PMF is sent to a PD for square-law detection, the photocurrent at the output of the PD is

$$\begin{aligned} I(t) &\propto \left|E'_x(t)\right|^2 + \left|E'_y(t)\right|^2 \\ &\approx 2 + \left\{\cos\left[\kappa u(t) + \phi_0\right] - \cos\left[\kappa u(t-\tau) + \phi_0\right]\right\} \end{aligned} \tag{15}$$

To generate an UWB monocycle, we set $\phi_0 = \pm\pi/2$. (15) can be then re-written as

$$I(t) \propto 2 \pm \left\{\sin\left[\kappa u(t)\right] - \sin\left[\kappa u(t-\tau)\right]\right\} \tag{16}$$

For small signal modulation, κ is small, we have $\sin\left[\kappa u(t)\right] = \kappa u(t)$, then (16) is approximated

$$I(t) \propto 2 \pm \kappa\left[u(t) - u(t-\tau)\right] \tag{17}$$

As can be seen the output current is proportional to the first-order difference of the input Gaussian pulse. Again, if τ is sufficiently small, the first-order difference can be approximated as the first-order derivative. Therefore, the entire system is equivalent to a first-order differentiator and a Gaussian monocycle is generated if the input drive signal is a Gaussian pulse.

Substituting $\phi_0 = \pm\pi/2$ into (14), and adopting the assumption of small signal modulation, we have

$$\begin{bmatrix} E'_x(t) \\ E'_y(t) \end{bmatrix} \propto \begin{bmatrix} (1 \pm j)\left\{1 \pm \kappa u(t)/2\right\} \\ e^{j\omega_c \tau}(1 \mp j)\left\{1 \mp \kappa u(t-\tau)/2\right\} \end{bmatrix} \tag{18}$$

From (18), we can see that both $E'_x(t)$ and $E'_y(t)$ have a fixed phase. Therefore, the generated Gaussian monocycle is chirp free.

The optical spectrum of the generated Gaussian monocycle can be written as

$$\begin{aligned} \tilde{P}(\omega) &= \left|\tilde{E}'_x(\omega)\right|^2 + \left|\tilde{E}'_y(\omega)\right|^2 \\ &\approx 8\pi^2\delta(\omega - \omega_c) + \frac{\kappa^2}{2}\tilde{U}^2(\omega - \omega_c) \end{aligned} \tag{19}$$

As can be seen from (19), the optical spectrum of the generated UWB pulse consists of a spectrum line corresponding to the optical carrier and a power spectrum of the input Gaussian pulse.

A photonic microwave delay-line filter using two independent wavelengths to generate an UWB Gaussian monocycle [27]–[29] has an optical spectrum in the form of

$$\begin{aligned} \tilde{P}(\omega) &= \left|2\pi\delta(\omega - \omega_{c1}) + \frac{\kappa}{2}\tilde{U}(\omega - \omega_{c1})\right|^2 \\ &+ \left|2\pi\delta(\omega - \omega_{c2}) + \frac{\kappa}{2}\tilde{U}(\omega - \omega_{c2})\right|^2 \end{aligned} \tag{20}$$

where ω_{c1} and ω_{c2} are the angular frequencies of the two wavelengths.

Fig. 2 shows the optical spectra of a DSB-UWB, QSSB-UWB and GUWB monocycle pulse obtained by numerical evaluations of the derived analytical equations. In the simulation, the time-domain waveforms of the generated UWB pulses are set to be same. The 3-dB bandwidths for the DSB-UWB, QSSB-UWB and GUWB monocycle pulse are 13.3, 6.4 and 6. 8 GHz; or the 10-dB bandwidths are 18.1, 11.7 and 12.4 GHz. The DSB-UWB monocycle pulse has an optical bandwidth much wider than that of the QSSB-UWB and GUWB monocycle pulses, while the QSSB-UWB monocycle pulse occupies the narrowest optical bandwidth.

III. Propagation in an Optical Fiber

When an optical pulse $E(z,t)$ propagates in an optical fiber, the CD will introduce a phase shift to each optical frequency component and accordingly the shape of the pulse will be changed. When propagating in an optical fiber, $E(z,t)$ satisfies the following linear partial differential equation [39]

$$j\frac{\partial E(z,t)}{\partial z} = \frac{\beta_2}{2}\frac{\partial^2 E(z,t)}{\partial t^2} \tag{21}$$

where β_2 is the group-velocity dispersion coefficient of the fiber and z is transmission distance along the fiber. The fiber loss is not considered in our model since it can be easily compensated by an erbium-doped fiber amplifier. Eq. (21) is readily solved by using the Fourier-transform method. The solution is given by

$$\tilde{E}(z,\omega) = \tilde{E}(0,\omega)\exp\left(\frac{j}{2}\beta_2\omega^2 z\right) \tag{22}$$

Since $\tilde{E}(0,\omega)$ for the optical DSB-UWB, QSSB-UWB and GUWB monocycle pulses is different, the transmission performance of these pulses in an optical fiber would be different.

A. DSB-UWB Monocycle Pulse

For a DSB-UWB monocycle pulse, the optical field at point z along the optical fiber is given by

$$\begin{aligned} \tilde{E}(z,\omega) &\approx 2\pi(1 \pm j)\delta(\omega - \omega_c) \\ &- (j \pm 1)\frac{\kappa}{2}\tilde{W}(\omega - \omega_c)\exp\left[\frac{j}{2}\beta_2(\omega - \omega_c)^2 z\right] \end{aligned} \tag{23}$$

In obtaining (23),$\omega_c \gg \omega - \omega_c$ is considered and $(\omega - \omega_c)^2 \approx \omega^2 - \omega_c^2$ is assumed. Converting (23) to the time domain, we obtain

$$E(z,t) = \exp\left(j\omega_c t\right)(1 \pm j)\left[1 \mp \frac{\kappa}{2}w_1(z,t)\right] \tag{24}$$

where

$$w_1(z,t) = -\frac{T_0^2 t\exp(1/2)}{\left(T_0^2 - j\beta_2 z\right)^{3/2}}\exp\left[-\frac{t^2}{2\left(T_0^2 - j\beta_2 z\right)}\right] \tag{25}$$

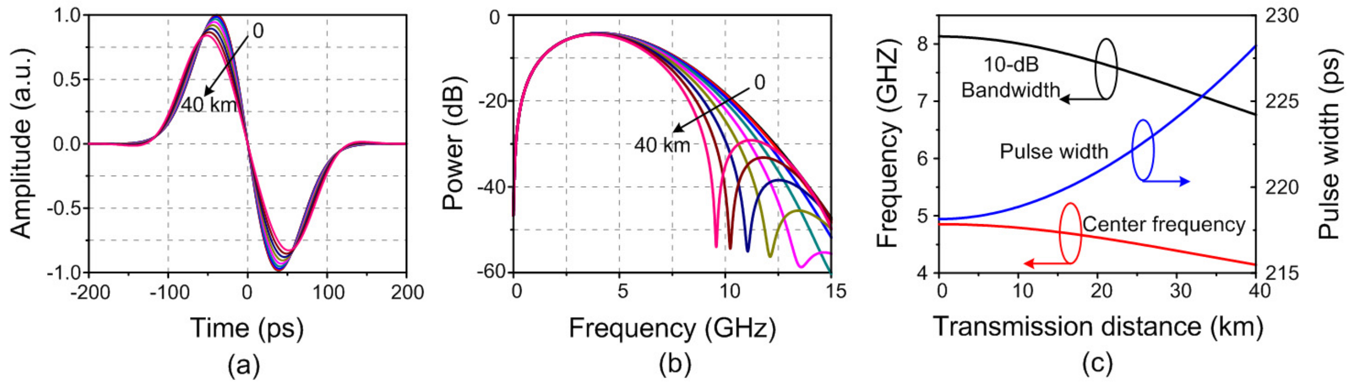

Fig. 3. Evolution of the optical DSB-UWB monocycle pulse with transmission distance varying from 0 to 40 km with an interval of 5 km. (a) waveforms, and (b) power spectra. (c) Evolution of the 10-dB bandwidth, center frequency and pulse width.

If $E(z,t)$ in (24) is applied to a PD for square-law detection, the photocurrent at the output of the PD is

$$I(z,t) \propto 1 \mp \kappa\left[\varepsilon_1(z)\cos\theta(z,t) + \varepsilon_2(z)\sin\theta(z,t)\right] w_2(z,t) \quad (26)$$

where

$$w_2(z,t) = -\frac{T_0^2 t\exp(1/2)}{\left(T_0^4+\beta_2^2z^2\right)^{3/2}}\exp\left[-\frac{t^2T_0^2}{2\left(T_0^4+\beta_2^2z^2\right)}\right] \quad (27)$$

$$\varepsilon_1(z) = -\frac{\beta_2 z\left(3T_0^4-\beta_2^2z^2\right)}{\left[2\left(T_0^4+\beta_2^2z^2\right)^{3/2}-2T_0^6+6T_0^2\beta_2^2z^2\right]^{1/2}} \quad (28)$$

$$\varepsilon_2(z) = \frac{1}{2}\left[2\left(T_0^4+\beta_2^2z^2\right)^{3/2}-2T_0^6+6T_0^2\beta_2^2z^2\right]^{1/2} \quad (29)$$

$$\theta(z,t) = \frac{t^2\beta_2 z}{2\left(T_0^4+\beta_2^2z^2\right)} \quad (30)$$

Compared (26) with (4), the dispersion of the optical fiber introduces a time-varied coefficient to the Gaussian monocycle, which would slightly change the profile of the waveform. As an example, we evaluate the evolution of an UWB pulse traveling in a standard single mode fiber (SMF, $\beta_2 \approx -21.7\text{ps}^2/\text{km}$). Fig. 3 shows the transmission performance of an optical DSB-UWB monocycle pulse traveling in a SMF. The results in Fig. 3(a) and (b) are obtained for the UWB pulse traveling in an SMF with a distance of 0, 5, 10, $\cdots$, 40 km. From Fig. 3(a) we can see that the temporal shape of the Gaussian monocycle slightly deviates from its original shape when propagating along the SMF. The pulse width, which is defined as the time interval between 10% the positive peak and 10% the negative peak, increases with z, from 216 ps at 0 km to 226 ps at 40 km, as can be seen from Fig. 3(c). Since the original pulse is chirp free, the increase of the pulse width would cause a decrease of the peak amplitude. The power spectrum of the UWB signal is given as $\tilde{\mathcal{F}}\{I(z,t)\}$. As can be seen from Fig. 3(b), the power of the high frequency components are reduced due to the low-pass equivalent filtering resulted from the dispersion medium [40]. According to [40], ideally the depth of the notches in Fig. 3(b) should be infinite. In our analysis, however, we have performed a first-order approximation since small signal modulation is employed, so the depth of the notches is finite. The 10-dB bandwidth is decreased from 8.22 GHz to 6.80 GHz, as can be seen from Fig. 3(c). Because the dispersion has less impact on the lower frequency components, the center frequency is shifted from 4.91 to 4.17 GHz.

B. QSSB-UWB Monocycle Pulse

Using a similar mathematical treatment as used in deriving (24), we obtain an expression for the optical field of a QSSB-UWB monocycle at point z along the optical fiber

$$E(z,t) \approx \exp(j\omega_c t)\left\{(1\pm j) + \frac{\kappa}{2}\left[ju_1(z,t-\tau) \mp u_1(z,t)\right]\right\} \quad (31)$$

where

$$u_1(z,t) = \frac{T_0}{\sqrt{T_0^2 - j\beta_2 z}}\exp\left[-\frac{t^2}{2\left(T_0^2-j\beta_2 z\right)}\right] \quad (32)$$

The photocurrent after optical to electrical conversion at a PD has the form

$$I^+(z,t) \approx 2 + \kappa A_2(z,t-\tau)u_2(z,t-\tau) - \kappa A_1(z,t)u_2(z,t) \quad (33)$$

$$I^-(z,t) \approx 2 - \kappa A_1(z,t-\tau)u_2(z,t-\tau) + \kappa A_2(z,t)u_2(z,t) \quad (34)$$

where

$$u_2(z,t) = -\frac{T_0}{\left(T_0^4+\beta_2^2z^2\right)^{1/2}}\exp\left[-\frac{t^2T_0^2}{2\left(T_0^4+\beta_2^2z^2\right)}\right] \quad (35)$$

$$A_1(z,t) = \left[\frac{\beta_2 z}{\eta(z)} - \frac{\eta(z)}{2}\right]\cos\theta(z,t) + \left[\frac{\beta_2 z}{\eta(z)} + \frac{\eta(z)}{2}\right]\sin\theta(z,t) \quad (36)$$

$$A_2(z,t) = \left[\frac{\beta_2 z}{\eta(z)} + \frac{\eta(z)}{2}\right]\cos\theta(z,t) - \left[\frac{\beta_2 z}{\eta(z)} - \frac{\eta(z)}{2}\right]\sin\theta(z,t) \quad (37)$$

In the above expressions

$$\eta(z) = \sqrt{2\sqrt{T_0^4+\beta_2^2z^2} - 2T_0^2} \quad (38)$$

As can be seen from (33) and (34), the UWB pulse after transmission over a dispersion medium has a similar

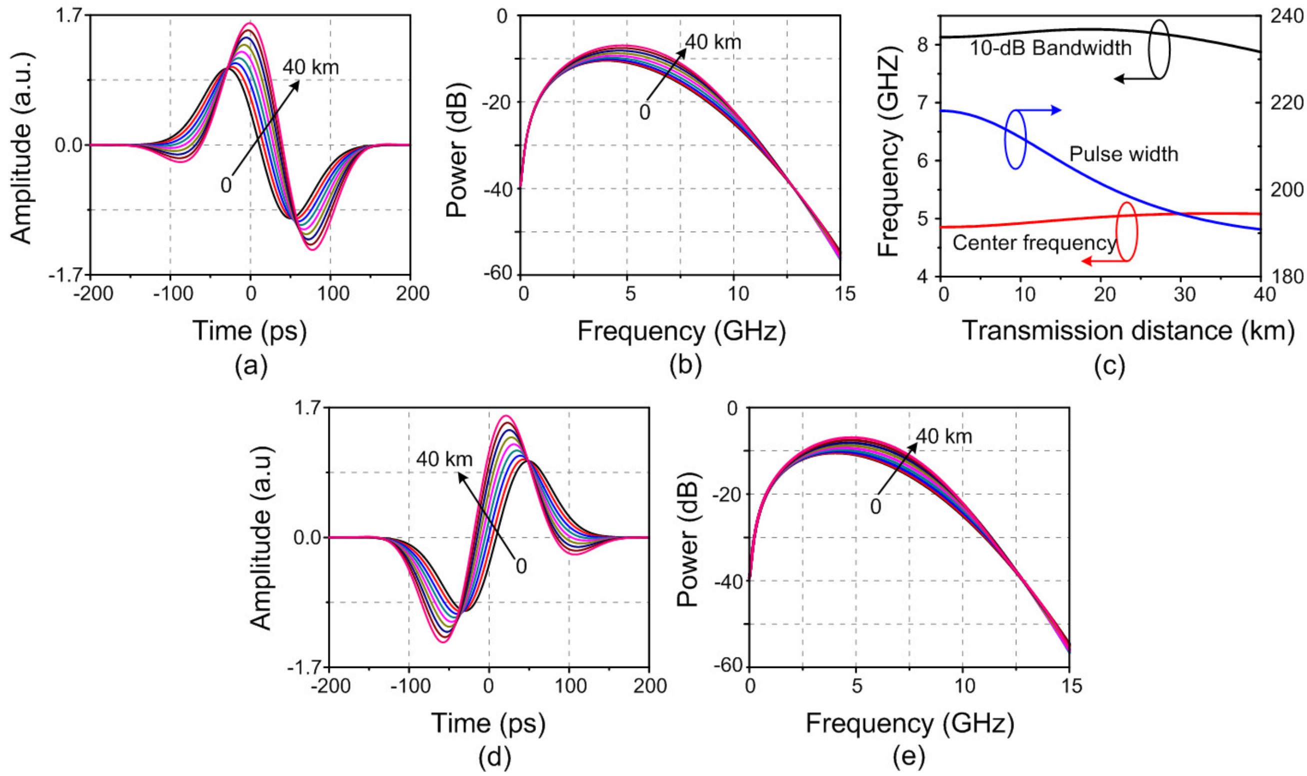

Fig. 4. Evolution of the optical QSSB-UWB monocycle pulse with transmission distance varying from 0 to 40 km with an interval of 5 km. (a), (d) waveforms, and (b), (e) power spectra. (c) Evolution of the 10-dB bandwidth, center frequency and pulse width.

expression as the original Gaussian monocycle, that is, the pulse is the difference of two time-delayed Gaussian pulses. However, the CD of the fiber introduces two different time-varied coefficients A_1 and A_2 to the two Gaussian pulses, which gives an amplitude imbalance to the two Gaussian pulses. As a result, the obtained UWB monocycle pulse would have two different peak amplitudes in the positive and negative parts. In addition, the pulse width T_1 of the Gaussian pulse $u_1(z,t)$ increases with z, which can be expressed as

$$T_1(z) = \sqrt{T_0^2 + (\beta_2 z/T_0)^2} \tag{39}$$

Because the expressions (33) and (34) for the pulses with negative and positive polarities are different, the pulses with different polarities may have a different time shift in the transmission, which is not desirable for some modulation schemes, such as BPM.

Fig. 4 shows the evolution of the QSSB-UWB monocycle with z in the time domain and in the frequency domain. In the time domain, the UWB pulse after transmission deviates from the shape of an ideal Gaussian monocycle. The power of the pulse increases with the transmission distance because the residual PM is converted to IM when the pulse is transmitted in the optical fiber (considering that the initial pulse is chirped). Because the pulse chirp is compensated by the fiber dispersion, the pulse width decreases with z, from 216 ps at 0 km to 191 ps at 40 km, as can be seen from Fig. 4(c). In the frequency domain, the peak power in the spectrum is increased and is shifted to a higher frequency. The 10-dB bandwidth is firstly increased since the original chirp is compensated by the fiber CD, and then decreased since the chirp introduced by the fiber CD is larger than the initial chirp. The total center frequency shift is less than 0.4 GHz and the change of the 10-dB bandwidth is smaller than 0.25 GHz for a transmission distance of less than 40 km. For UWB communications, the spectral profile of an UWB pulse that satisfies the spectral mask defined by the FCC is more important. Since the center frequency and the 10-dB bandwidth is only slightly changed with the transmission distance, the QSSB-UWB optical pulse can be considered to have a good tolerance to the fiber CD. In addition, the increase of the power with the transmission distance can be used to compensate partially for the transmission loss in the optical fiber. Furthermore, as shown in Fig. 4(a) and (d) the pulses with negative and positive polarities have an undesirable time shift in the transmission. But the power spectra are the same, as depicted in Fig. 4(b) and (e).

C. GUWB Monocycle Pulse

When the optical signal shown in (18) is transmitted over an optical fiber, the two orthogonally polarized light waves traveling along the two principal axes of the PMF will be affected by the CD. The optical filed at point z along the fiber is given by

$$\begin{bmatrix} E'_x \\ E'_y \end{bmatrix} \propto \begin{bmatrix} (1 \pm j)\{1 \pm \kappa u_1(t)/2\} \\ e^{j\omega_c \tau}(1 \mp j)\{1 \mp \kappa u_1(t-\tau)/2\} \end{bmatrix} \tag{40}$$

When the optical signal is sent to a PD, we obtain the photocurrent at the output of the PD,

$$I(z,t) \approx 2 \pm \kappa \left[B(z,t-\tau)u_2(z,t-\tau) - B(z,t)u_2(z,t)\right] \tag{41}$$

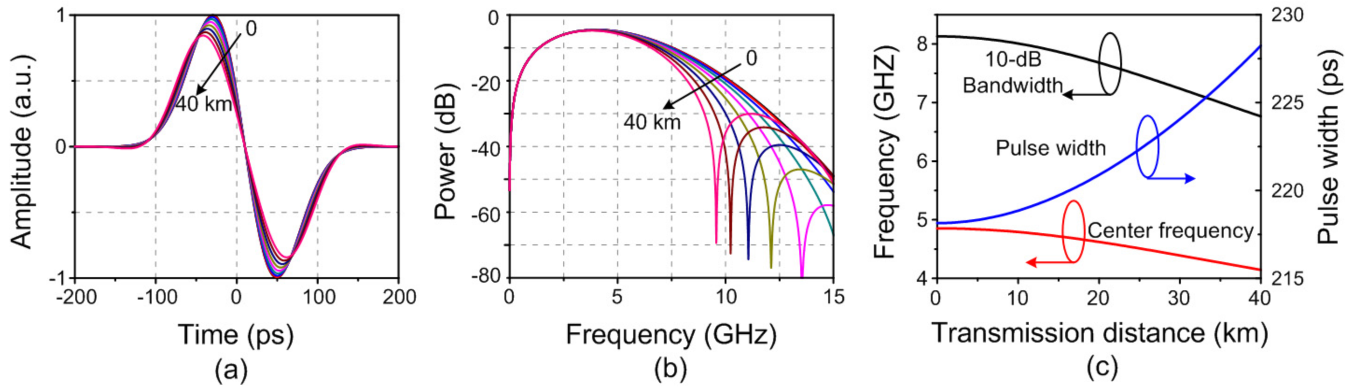

Fig. 5. Evolution of the optical GUWB monocycle pulse with transmission distance varying from 0 to 40 km with an interval of 5 km. (a) waveforms, and (b) power spectra. (c) Evolution of the 10-dB bandwidth, center frequency and pulse width.

where

$$B(z,t) = \frac{\beta_2 z}{\eta(z)}\cos\theta(z,t) + \frac{\eta(z)}{2}\sin\theta(z,t) \tag{42}$$

For a two-tap photonic microwave delay-line filter using two wavelengths, the expression for $B(z,t)$ is the same as in (42) except that β_2 has to be changed to $\beta_2(\lambda)$.

Fig. 5 shows the simulated results for the transmission of a GUWB monocycle pulse over a SMF. The GUWB monocycle almost maintains its shape when propagating in the fiber. The pulse width has a slight increase after transmission, from 218 ps at 0 km to 228 ps at 40 km. The power of the UWB pulse decreases with z. In the frequency domain, the high frequency components are compressed while the low frequency components are almost kept unchanged. From Fig. 5(c), the 10-dB bandwidth decreases from 8.13 to 6.76 GHz, and the center frequency is shifted from 4.85 to 4.14 GHz. Comparing Fig. 5 with Fig. 3, we can find that the transmission performance of the GUWB monocycle is very similar to that of a DSB-UWB pulse. This is because that a GUWB monocycle is the combination of two incoherent time-delayed optical signals. Both of the time-delayed signals would be degraded by the CD when they are transmitted in the optical fiber. As a result, the transmission performance of the combined signal is equivalent to that of a single optical signal occupying a wider optical bandwidth.

IV. PSD Analysis

The PSD of a typical electrical UWB signal with BPM and PPM has been given in the literature [32]–[38]. In the work reported in [32]–[38], however, the expressions for pulses to represent '0' and '1' are the same or have a simple relationship. Based on the study, the expression for the pulse to represent '0' is different from the one for a UWB pulse to represent '1' when the UWB signals are transmitting in an optical fiber. As a result, a more general model must be established to include the fiber transmission effects. To do so, we represent a data-modulated UWB signal by

$$x(t) = \sum_{n=-\infty}^{\infty}\left[(1-a_n)f_0(t-nT-\mu_n) + a_n f_1(t-nT-\mu_n)\right] \tag{43}$$

where $\{a_n\}$ is a binary independent and identically distributed (i.i.d.) random sequence with a probability density function (PDF) $P(a_n = 1) = p$, T is the bit period, f_0 and f_1 are the waveforms representing bits '0' and '1', respectively, and μ_n is the TH time shift, which is uniformly distributed in $[-\Delta, \Delta]$. For modulation schemes such as OOK, BPM and PPM, f_0 and f_1 are present in Table I.

TABLE I
f_0 and f_1 for Different Modulation Schemes

	f_0	f_1
OOK	0	$I(z,t)$
BPM	$I^-(z,t)$	$I^+(z,t)$
PPM	$I(z,t-T_b)$	$I(z,t)$

$I(z,t)$ is the expression of the electrical UWB pulse obtained at the output port of the PD. $I^+(z,t)$ and $I^-(z,t)$ represent pulses with positive and negative polarities, respectively.

In the appendix, the PSD for the signal $x(t)$ is expressed as

$$S(\omega) = S_C(\omega) + S_D(\omega) \tag{44}$$

where $S_C(\omega)$ and $S_D(\omega)$ denote the continuous part and the discrete part of the PSD, respectively, which are given by

$$\begin{aligned} S_C(\omega) =& \frac{\left|\tilde{F}_0(\omega)\right|^2}{T}\left[(1-p)-(1-p)^2\mathrm{sinc}^2\left(\frac{\omega\Delta}{2}\right)\right] \\ &+ \frac{\left|\tilde{F}_1(\omega)\right|^2}{T}\left[p-p^2\mathrm{sinc}^2\left(\frac{\omega\Delta}{2}\right)\right] \\ &- \frac{\left|\tilde{F}_0(\omega)\tilde{F}_1^*(\omega)+\tilde{F}_0^*(\omega)\tilde{F}_1(\omega)\right|}{T}p(1-p)\mathrm{sinc}^2\left(\frac{\omega\Delta}{2}\right) \end{aligned} \tag{45}$$

$$\begin{aligned} S_D(\omega) =& \frac{1}{T^2}\sum_{n=-\infty}^{\infty}\delta\left(\omega-\frac{2\pi n}{T}\right)\left\{\left|\tilde{F}_0(\omega)\right|^2(1-p)^2\mathrm{sinc}^2\left(\frac{\omega\Delta}{2}\right)\right. \\ &+ \left|\tilde{F}_1(\omega)\right|^2 p^2\mathrm{sinc}^2\left(\frac{\omega\Delta}{2}\right) \\ &\left.+\left[\tilde{F}_0(\omega)\tilde{F}_1^*(\omega)+\tilde{F}_0^*(\omega)\tilde{F}_1(\omega)\right]p(1-p)\mathrm{sinc}^2\left(\frac{\omega\Delta}{2}\right)\right\} \end{aligned} \tag{46}$$

Because an UWB antenna can be considered as a differentiation block in the time domain, the radiated PSD of the UWB signal is then written as

$$S_{\mathrm{R}}(\omega) \propto \omega^2 S(\omega) \tag{47}$$

As can be seen from (44)-(47), the radiated PSD of an UWB signal is determined by five parameters, i.e., $\tilde{F}_0(\omega)$, $\tilde{F}_1(\omega)$, T, p and Δ. Since T, p and Δ are time invariant in transmission, and and can be obtained by the Fourier transform of the signals in (26), (33), (34) or (41) using the fast Fourier transform algorithm, (47) can be numerically calculated.

In this section, the radiated PSD of an OOK, BPM and PPM UWB monocycle signal in transmission is calculated by setting $p = 0.5$ and $T = 1$ ns, i.e., with a bit rate equal to 1 Gbit/s. It should be noted if f_0 and f_1 have different shapes or different amplitude, (43) is an expression for a pulse-shape modulated (PSM) or pulse-amplitude modulated (PAM) signal. Thus, (44) to (47) can also applied to study the radiated PSD of a PSM and PAM signal.

A. On-Off Keying

For OOK modulation scheme, f_0 equals to 0. Because of the blank transmission in case of bit '0' and because it could create further problems for synchronization [4], OOK cannot take advantage of TH. Thus, $\Delta = 0$. (47) can then be simplified to

$$S_{\mathrm{R\text{-}OOK}} \propto \frac{\omega^2 p \tilde{F}_1(\omega)}{T}\left[(1-p) + \frac{p}{T}\sum_{n=-\infty}^{\infty}\delta\left(\omega - \frac{2\pi n}{T}\right)\right] \tag{48}$$

As can be seen from (48), the ratio of the powers for the discrete lines and the continuous points are $p/T(1-p)$. For $p = 0.5$ and $T = 1$ ns, this ratio is as large as 10^9. Fig. 6 shows the PSD of a radiated OOK UWB monocycle signal before transmission and after 20- and 40-km SMF transmission. As expected, the discrete lines are 90 dB larger than its continuous counterpart. The FCC-specified indoor spectral mask is also plotted. The powers of the initial UWB signals are controlled to satisfy the FCC mask. From Fig. 6, the high frequency components are reduced by fiber dispersion for the UWB signals based on DSB-UWB and GUWB monocycles, which would further reduce the total transmitted power from the antenna. On the contrary, the CD has a positive impact on the PSD of an UWB signal based on QSSB-UWB monocycles. The components in the 3.1-10.6 GHz band are enhanced, which would increase the total transmitted power. Comparably, QSSB-UWB monocycles are more suitable for UWBoF system with OOK modulation scheme.

B. Bi-Phase Modulation

For ideal BPM, the pulses shape (e.g., the AC term of $I(z,t)$) for '0' and '1' are inverted, i.e., $f_0 = -f_1$. Substituting this relation to (45) and (46), we obtain the radiated PSD, given by

$$S_{\mathrm{R\text{-}BPM}} = \frac{\omega^2\left|\tilde{F}_0(\omega)\right|^2}{T}\left[1-(1-2p)^2\mathrm{sinc}^2\left(\frac{\omega\Delta}{2}\right)\right] + \frac{\omega^2(1-2p)^2}{T^2}\sum_{n=-\infty}^{\infty}\left|\tilde{F}_0(\omega)\right|^2\mathrm{sinc}^2\left(\frac{\omega\Delta}{2}\right)\delta\left(\omega-\frac{2\pi n}{T}\right) \tag{49}$$

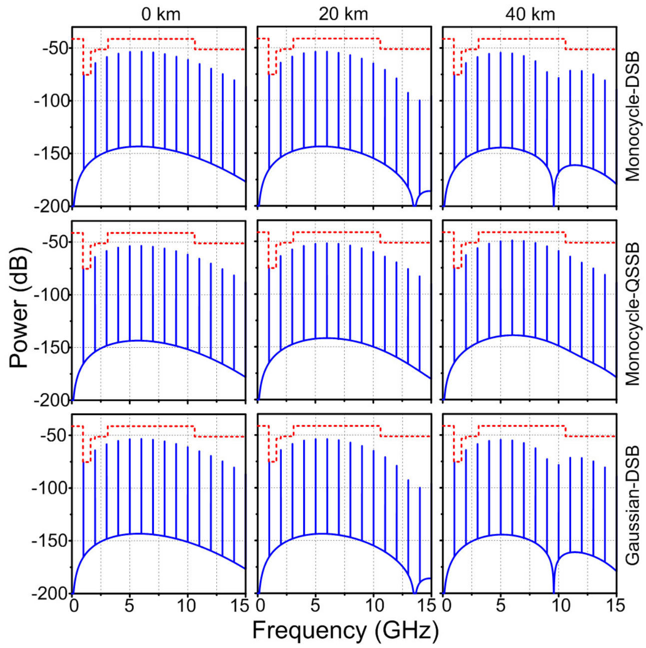

Fig. 6. Radiated PSD of OOK UWB signals based on DSB-UWB, QSSB-UWB and GUWB monocycles before transmission and after 20- and 40-km SMF transmission.

As can be seen from (49) $S_{\mathrm{R-BPM}}$ has the same expression as that for a BPM signal in [32]. If $p = 0.5$, the discrete part of the PSD equals to 0. After transmission over an optical fiber, the UWB signals based on the DSB-UWB and GUWB monocycles still maintain the relation $f_0 = -f_1$, as can be seen from the expressions shown in (24) and (41), so no new discrete lines are generated. However, from (33) and (34) there is a time shift for the QSSB-UWB monocycles with different polarities after transmission. As a result, f_0 does not equal to $-f_1$ and the discrete lines would be generated again. The calculated results for the PSD of a BPM UWB monocycle signal without TH are shown in Fig. 7. The initial UWB signal has no discrete lines in the PSD, which indicates that the total transmitted power from the antenna can be greatly increased as compared with the OOK modulation scheme. After 20- and 40-km SMF transmission, no new discrete lines appear in the PSD of the DSB-UWB and GUWB monocycle signals, while strong discrete lines are created again for the UWB signal based on the QSSB-UWB monocycles.

In a practical system, it is very hard to keep exactly $p = 0.5$. If p slightly deviates from 0.5, strong discrete lines would be present in the PSD of the initial UWB signals. For instance, we set $p = 0.55$ and calculate the PSD again. The results are shown in Fig. 8. For the initial signals, the discrete lines are 70 dB larger than its continuous counterpart. When transmitted in an optical fiber, this ratio is maintained for the UWB signals based on DSB-UWB and GUWB monocycles, while it is increased up to 19 dB after 20-km SMF transmission and is increased up to 31 dB after 40-km SMF transmission for the UWB signal based on QSSB-UWB monocycles. Since the strong discrete lines would present great interferences to other narrowband communication systems, the QSSB-UWB monocycles cannot be used in an UWBoF system with BPM. It should be noted that some optical UWB pulse generators

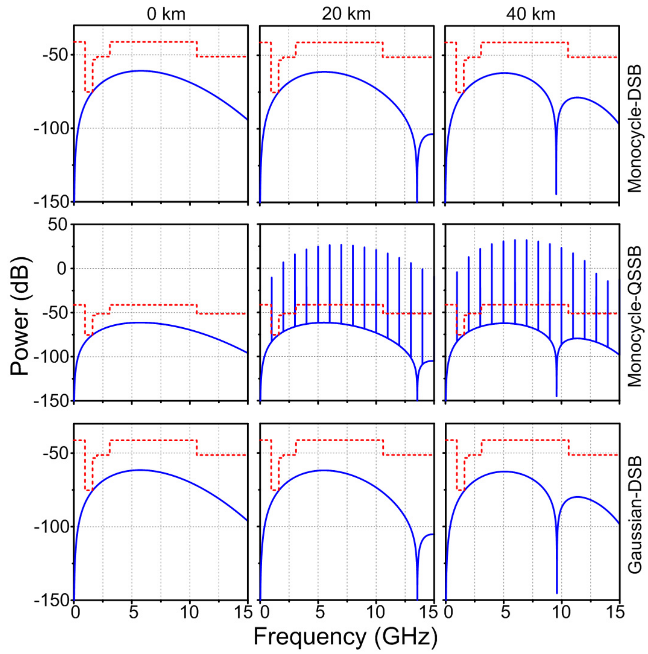

Fig. 7. Radiated PSD of BPM UWB signals based on DSB-UWB, QSSB-UWB and GUWB monocycles before transmission and after 20- and 40-km SMF transmission when $p = 0.5$.

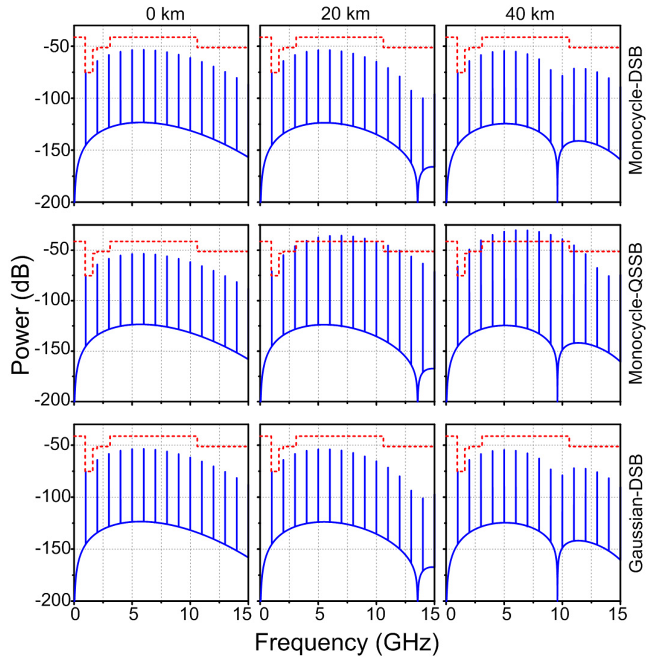

Fig. 8. Radiated PSD of BPM UWB signals based on DSB-UWB, QSSB-UWB and GUWB monocycles before transmission and after 20- and 40-km SMF transmission when $p = 0.55$.

would introduce an initial time shift to the UWB pulses with different polarities [30]. In that case, the time shift introduced by the fiber transmission may compensate in part the original time shift and thus have a positive impact on the system performance.

C. Pulse Position Modulation

For PPM, the pulses for ‘0’ and ‘1’ have a time shift of T_b, so we have

$$\tilde{F}_1(\omega) = \tilde{F}_0(\omega)\exp(j\omega T_b) \tag{50}$$

Substituting (50) into (45) and (46), we obtain

$$S_C(\omega) = \frac{\left|\tilde{F}_0(\omega)\right|^2}{T}\left\{1 - \mathrm{sinc}^2\left(\frac{\omega\Delta}{2}\right) \cdot \left[(1-p)^2 + p^2 - 2p(1-p)\cos(\omega T_b)\right]\right\} \tag{51}$$

$$S_D(\omega) = \frac{1}{T^2}\sum_{n=-\infty}^{\infty}\left|\tilde{F}_0(\omega)\right|^2 \mathrm{sinc}^2\left(\frac{\omega\Delta}{2}\right)\delta\left(\omega - \frac{2\pi n}{T}\right) \cdot \left[(1-p)^2 + p^2 + 2p(1-p)\cos(\omega T_b)\right] \tag{52}$$

As can be seen from (51) and (52), both the discrete and the continuous parts of the PSD are the power spectrum of an UWB pulse multiplied by a cosine-based function. Since a cosine function is periodic, there should be many notches with a spacing of $1/T_b$ in the PSD. In the calculation, we set $T_b = T/2$. Fig. 9 shows the radiated PSD of a PPM UWB monocycle signal without TH before transmission and after 20- and 40-km SMF transmission. Just as the case in OOK, the power of the high frequency components are reduced by the fiber dispersion for the UWB signals based on DSB-UWB and GUWB monocycles, while the components in the 3.1 to 10.6 GHz band are enhanced for the UWB signal based on QSSB-UWB monocycles. Therefore, QSSB-UWB monocycles have the best transmission performance in an UWBoF system with PPM.

In the above study, we only calculated the PSD for UWB signals without TH. It is known that the employment of TH can reduce the spectral lines in the PSD of an UWB signal, which can also minimize collisions between users in a multiple access system using a distinct pulse shift pattern for each user [4]. From (45) and (46), the impact of TH is related to the terms containing $\mathrm{sinc}^2(\omega\Delta/2)$. For the PPM signals, as can be seen from (51) and (52) the TH terms and $\tilde{F}_0(\omega)$ terms can be separated, so the impact of TH is independent of transmission distance. This feature is also applicable to a BPM signal based on DSB-UWB or GUWB monocycles (see (49)). The impact of TH on the PSD of such a signal would be the same as that in a wireless link, which has been sufficiently investigated [32]–[36]. For a BPM signal based on the QSSB-UWB monocycles, the TH terms and $\tilde{F}_0(\omega)$ terms cannot be separated. A numerical simulation is performed by setting $\Delta = 0.1$ ns. Fig. 10 shows the radiated PSD of a BPM UWB signal without (solid line) and with (dotted line) TH based on the QSSB-UWB monocycles after 20- and 40-km SMF transmission. To avoid overlap, in Fig. 10 the PSD of the TH UWB signal is manually shifted by 0.1 GHz. As can be seen, the notches in the continuous part are eliminated. Meanwhile, the power of the discrete lines is reduced up to 26 dB for the signal after 20-km SMF transmission and up to 28 dB for the signal after 40-km SMF transmission. However, the discrete lines are still too strong.

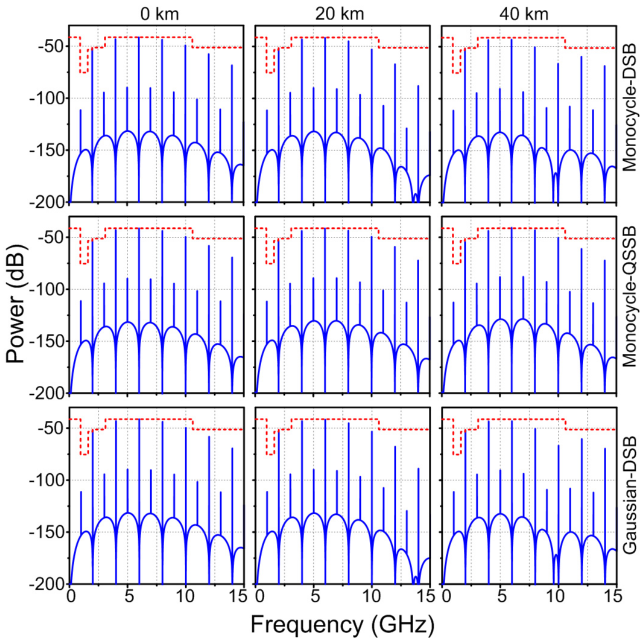

Fig. 9. Radiated PSD of PPM UWB signals based on DSB-UWB, QSSB-UWB and GUWB monocycles before transmission and after 20- and 40-km SMF transmission.

V. Conclusion

We have theoretically studied the transmission performance of UWB signals over optical fiber. The optical spectral properties of the DSB-UWB, QSSB-UWB, GUWB monocycles were analyzed. The DSB-UWB monocycle has an optical bandwidth much wider than that of the QSSB-UWB and GUWB monocycles, and the QSSB-UWB monocycle occupies the narrowest optical bandwidth. The impact of fiber dispersion on the waveforms and spectra of the Gaussian monocycles were studied. The transmission performance of the GUWB monocycle is very similar to that of a DSB-UWB pulse, while the QSSB-UWB monocycles were found to have a better tolerance to fiber dispersion. A general model to analyze the PSD of UWB signals was developed to investigate the transmission performance of data-modulated monocycle signals. The PSD of a monocycle-based UWB signal with OOK, BPM and PPM schemes was calculated. The UWB signals based on QSSB-UWB monocycles were found to be more suitable for an UWBoF system with OOK or PPM, while the UWB signals based on DSB-UWB or GUWB monocycles have better transmission performance for an UWBoF system with BPM.

Appendix A

Suppose that a data-modulated UWB signal is represented in the time domain by

$$x(t) = \sum_{n=-\infty}^{\infty} \left[(1-a_n)f_0(t-nT-\mu_n) + a_n f_1(t-nT-\mu_n)\right] \tag{A1}$$

where $\{a_n\}$ is a binary i.i.d. random sequence, μ_n is uniformly distributed in $[-\Delta, \Delta]$. The PSD of (A1) can be computed

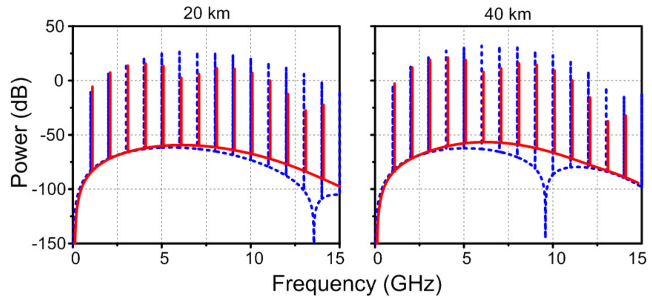

Fig. 10. Radiated PSD of a BPM UWB signal without (dashed line) and with (solid line) TH based on QSSB-UWB monocycles after 20- and 40-km SMF transmission when $p = 0.5$.

using the Wiener-Kinchine theorem as follows [35].

$$S(\omega) = \lim_{N\to\infty} \frac{1}{NT} E\left\{|X_N(\omega)|^2\right\} \tag{A2}$$

where E denotes the expectation, and

$$\begin{aligned} X_N(\omega) =& \tilde{F}_0(\omega)\sum_{n=1}^{N}(1-a_n)\exp\left[-j\omega(nT+\mu_n)\right] \\ &+ \tilde{F}_1(\omega)\sum_{n=1}^{N} a_n \exp\left[-j\omega(nT+\mu_n)\right] \end{aligned} \tag{A3}$$

where $\tilde{F}_0(\omega)$ and $\tilde{F}_1(\omega)$ are the Fourier transform of f_0 and f_1, respectively. Then,

$$\begin{aligned} S(\omega) &= \lim_{N\to\infty} \frac{1}{NT} E\left\{X_N(\omega)\cdot X_N^*(\omega)\right\} \\ &= \lim_{N\to\infty} \frac{1}{NT}\left[Y_1(\omega) + Y_2(\omega) + Y_3(\omega)\right] \end{aligned} \tag{A4}$$

where

$$\begin{aligned} Y_1(\omega) =& |\tilde{F}_0(\omega)|^2 \sum_{n=1}^{N}\sum_{m=1}^{N} E\left\{(1-a_n)(1-a_m)\exp\left[-j\omega(n-m)T\right]\right\} \\ &\cdot E\left\{\exp\left[-j\omega(\mu_n-\mu_m)\right]\right\} \end{aligned} \tag{A5}$$

$$\begin{aligned} Y_2(\omega) =& |\tilde{F}_1(\omega)|^2 \sum_{n=1}^{N}\sum_{m=1}^{N} E\left\{a_n a_m \exp\left[-j\omega(n-m)T\right]\right\} \\ &\cdot E\left\{\exp\left[-j\omega(\mu_n-\mu_m)\right]\right\} \end{aligned} \tag{A6}$$

$$\begin{aligned} Y_3(\omega) =& \left[\tilde{F}_0(\omega)\tilde{F}_1^*(\omega) + \tilde{F}_0^*(\omega)\tilde{F}_1(\omega)\right] \\ &\cdot \sum_{n=1}^{N}\sum_{m=1}^{N} E\left\{a_n(1-a_m)\exp\left[-j\omega(n-m)T\right]\right\} \\ &\cdot E\left\{\exp\left[-j\omega(\mu_n-\mu_m)\right]\right\} \end{aligned} \tag{A7}$$

In the above expressions

$$\begin{aligned} &E\left\{\exp\left[-j\omega(\mu_n-\mu_m)\right]\right\} \\ &= \begin{cases} 1 & m = n \\ \frac{1}{4\Delta^2}\int_{-\Delta}^{\Delta} dx \int_{-\Delta}^{\Delta} dy \exp\left[-j\omega(x-y)\right] = \operatorname{sinc}^2\left(\frac{\omega\Delta}{2}\right) & m \neq n \end{cases} \end{aligned} \tag{A8}$$

Assume the PDF of a_n is

$$P(a_n) = \begin{cases} p & a_n = 1 \\ 1-p & a_n = 0 \end{cases} \tag{A9}$$

we can obtain

$$E\{a_n a_m\} = \begin{cases} p & m = n \\ p^2 & m \neq n \end{cases} \tag{A10}$$

$$E\{(1-a_n)(1-a_m)\} = \begin{cases} 1-p & m = n \\ (1-p)^2 & m \neq n \end{cases} \tag{A11}$$

$$E\{a_n(1-a_m)\} = \begin{cases} 0 & m = n \\ p(1-p) & m \neq n \end{cases} \tag{A12}$$

Then

$$\begin{aligned} &\sum_{n=1}^{N}\sum_{m=1}^{N} E\left\{(1-a_n)(1-a_m)\exp\left[-j\omega(n-m)T\right]\right\} \\ &\cdot E\left\{\exp\left[-j\omega(\mu_n-\mu_m)\right]\right\} \\ &= \sum_{n=1}^{N}\exp(-j\omega nT)\sum_{m=1}^{N} E\left\{(1-a_n)(1-a_m)\right\}\exp(j\omega mT) \\ &\cdot E\left\{\exp\left[-j\omega(\mu_n-\mu_m)\right]\right\} \end{aligned} \tag{A13}$$

In the above expression

$$\begin{aligned} &\sum_{m=1}^{N} E\left\{(1-a_n)(1-a_m)\right\}\exp(j\omega mT)E\left\{\exp\left[-j\omega(\mu_n-\mu_m)\right]\right\} \\ &= (1-p)\exp(j\omega nT) + \sum_{m=1, m\neq n}^{N}(1-p)^2\exp(j\omega mT)\mathrm{sinc}^2\left(\frac{\omega\Delta}{2}\right) \\ &= \left[(1-p)-(1-p)^2\mathrm{sinc}^2\left(\frac{\omega\Delta}{2}\right)\right]\exp(j\omega nT) \\ &+ (1-p)^2\mathrm{sinc}^2\left(\frac{\omega\Delta}{2}\right)\sum_{m=1}^{N}\exp(j\omega mT) \end{aligned} \tag{A14}$$

Hence, $Y_1(\omega)$ is simplified to

$$\begin{aligned} Y_1(\omega) &= N|\tilde{F}_0(\omega)|^2\left[(1-p)-(1-p)^2\mathrm{sinc}^2\left(\frac{\omega\Delta}{2}\right)\right] \\ &+ |\tilde{F}_0(\omega)|^2\sum_{n=1}^{N}\exp(j\omega nT)(1-p)^2\mathrm{sinc}^2\left(\frac{\omega\Delta}{2}\right) \\ &\cdot\frac{1-\exp(j\omega NT)}{1-\exp(j\omega T)} \\ &= N|\tilde{F}_0(\omega)|^2\left[(1-p)-(1-p)^2\mathrm{sinc}^2\left(\frac{\omega\Delta}{2}\right)\right] \\ &+ (1-p)^2\mathrm{sinc}^2\left(\frac{\omega\Delta}{2}\right)|\tilde{F}_0(\omega)|^2\left[\frac{1-\exp(j\omega NT)}{1-\exp(j\omega T)}\right]^2 \end{aligned} \tag{A15}$$

Using a similar mathematical treatment as used in deriving (A15), the simplified expressions for $Y2(\omega)$ and $Y3(\omega)$ can also be obtained. Substituting them into (A4), we obtain

$$S(\omega) = S_{\mathrm{C}}(\omega) + S_{\mathrm{D}}(\omega) \tag{A16}$$

where $S_{\mathrm{C}}(\omega)$ and $S_{\mathrm{D}}(\omega)$ denotes the continuous part and the discrete part of the PSD, respectively, which are represented by

$$\begin{aligned} S_{\mathrm{C}}(\omega) &= \frac{\left|\tilde{F}_0(\omega)\right|^2}{T}\left[(1-p)-(1-p)^2\mathrm{sinc}^2\left(\frac{\omega\Delta}{2}\right)\right] \\ &+ \frac{\left|\tilde{F}_1(\omega)\right|^2}{T}\left[p-p^2\mathrm{sinc}^2\left(\frac{\omega\Delta}{2}\right)\right] \\ &- \frac{\left|\tilde{F}_0(\omega)\tilde{F}_1^*(\omega)+\tilde{F}_0^*(\omega)\tilde{F}_1(\omega)\right|}{T}p(1-p)\mathrm{sinc}^2\left(\frac{\omega\Delta}{2}\right) \end{aligned} \tag{A17}$$

$$\begin{aligned} S_{\mathrm{D}}(\omega) &= \frac{1}{T^2}\sum_{n=-\infty}^{\infty}\delta\left(\omega-\frac{2\pi n}{T}\right)\left\{\left|\tilde{F}_0(\omega)\right|^2(1-p)^2\mathrm{sinc}^2\left(\frac{\omega\Delta}{2}\right)\right. \\ &+ \left|\tilde{F}_1(\omega)\right|^2 p^2\mathrm{sinc}^2\left(\frac{\omega\Delta}{2}\right) \\ &\left.+ \left[\tilde{F}_0(\omega)\tilde{F}_1^*(\omega)+\tilde{F}_0^*(\omega)\tilde{F}_1(\omega)\right]p(1-p)\mathrm{sinc}^2\left(\frac{\omega\Delta}{2}\right)\right\} \end{aligned} \tag{A18}$$

In obtaining (A17) and (A18), the following relationship is adopted

$$\lim_{N\to\infty}\frac{1}{NT}\left(\frac{\sin\omega NT}{\omega T}\right)^2 = \frac{1}{T^2}\sum_{n=-\infty}^{\infty}\delta\left(\omega-\frac{2\pi n}{T}\right) \tag{A19}$$

References

[1] G. R. Aiello and G. D. Rogerson,“Ultra-wideband wireless systems,” *IEEE Microwave*, vol. 4, no. 2, pp. 36-47, Jun. 2003.

[2] D. Porcino and W. Hirt, “Ultra-wideband radio technology: Potential and challenges ahead,” *IEEE Commun. Mag.*, vol. 41, no. 7, pp. 66-74, Jul. 2003.

[3] M. Ghavami, L. B. Michael, and R. Kohno, *Ultra Wideband Signals and Systems in Communication Engineering*. West Sussex, U.K.: Wiley, 2004.

[4] I. Oppermann, M. Hämäläinen and J. Iinatti, *UWB theory and applications*. Chichester, U.K.: Wiley, 2004.

[5] J. P. Yao, F. Zeng, and Q. Wang, “Photonic generation of ultrawideband signals,” *J. Lightwave Technol.*, vol. 25, no. 11, pp. 3219-3235, Nov. 2007.

[6] C. M. Tan, L. C. Ong, M. L. Yee, B. Luo, and P. K. Tang, “Direct transmission of ultra wide band signals using single mode radio-overfiber system,” in *Proc. MW Conf.*, Dec. 2005, vol. 2.

[7] C. S. Lim, M. L. Yee, and C. S. Ong, “Performance of transmission of ultra wideband signals using radio-over-fiber system,” in *Proc. ITS Tele. Conf.*, pp. 250-253, Jun. 2006.

[8] L. C. Ong, M. L. Yee, and B. Luo, “Transmission of ultra wideband signals through radio-over-fiber systems,” in *Proc. LEOS 2006*, pp. 522-523, Oct. 2006.

[9] R. Llorente, T. Alves, M. Morant, M. Beltran, J. Perez, A. Cartaxo, and J. Marti, “Ultra-wideband radio signals distribution in FTTH networks,” *IEEE Photon. Technol. Lett.*, vol. 20, no. 10, pp. 945-947, May 2008.

[10] M. P. Thakur, T. J. Quinlan, C. Bock, S. D. Walker, M. Toycan, S. E. M. Dudley, D. W. Smith, A. Borghesani, D. Moodie, M. Ran, and Y. Ben-Ezra, “480-Mbps, bi-directional, ultra-wideband radio-over-fiber transmission using a 1308/1564-nm reflective electro-absorption transducer and commercially available VCSELs,” *J. Lightwave Technol.*, vol. 27, no. 3, pp. 266-272, Feb. 2009.

[11] T.B. Gibbon, X. B. Yu, R. Gamatham, N. G. Gonzalez and I. T. Monroy, “3.125 Gb/s impulse radio UWB over fiber transmission,” in *Proc.ECOC 2009*, paper P 6.01.

[12] S. L. Pan and J. P. Yao, “Photonic generation and transmission of UWB signals with on-off keying and bi-phase modulation schemes,” in *Proc. OECC 2009*, paper TuH2.

[13] S. L. Pan and J. P. Yao, “Photonic generation of chirp-free UWB signals for UWB over fiber applications,” in *Proc. MWP 2009*, Valencia, Spain, Oct. 14-16, 2009, paper Th3.7.

[14] A. Kaszubowska-Anandarajah and L.P. Barry, “UWB system based on gain-switched laser,” in *Proc. MWP 2006*, 3-6 Oct. 2006.

[15] M. Hanawa, K. Mori, K. Nakamura, A. Matsui, Y. Kanda, and K. Nonaka, "Dispersion tolerant UWB-IR-over-fiber transmission under FCC indoor spectrum mask," in *Proc. OFC 2009*, Paper OTuJ3.

[16] M. Jazayerifar, B. Cabon, and J. A. Salehi, "Transmission of multi-band OFDM and impulse radio ultra-wideband signals over single mode fiber," *J. Lightwave Technol.*, vol. 26, no. 13-16, pp. 2594-2603, Jul-Aug. 2008.

[17] M. L. Yee, L. C. Ong, C. K. Sim, B. Luo, and A. Alphones, "Low-cost Radio-Over-Fiber in-building distribution network for WLAN, UWB and digital TV broadcasting," in *Proc. Asia-Pacific Microwave Conference 2006*, pp. 95-98, 2006.

[18] C. Wang, F. Zeng, and J. P. Yao, "All-fiber ultrawideband pulse generation based on spectral-shaping and dispersion-induced frequency-to-time conversion," *IEEE Photon. Technol. Lett.*, vol. 19, no. 3, pp. 137-139, Feb. 2007.

[19] M. Abtahi, M. Mirshafiei, S. LaRochelle, and L. A. Rusch, "All-optical 500-Mb/s UWB transceiver: an experimental demonstration," *J. Lightwave Technol.*, vol. 26, no. 15, pp. 2795-2802, Aug. 2008.

[20] S. L. Pan and J. P. Yao, "An optical UWB pulse generator for flexible modulation format," *IEEE Photon. Technol. Lett.*, vol. 21, no. 19, pp. 1381-1383, Sep. 2009.

[21] F. Zeng and J. P. Yao, "Ultrawideband impulse radio signal generation using a high-speed electrooptic phase modulator and a fiber-Bragg-grating-based frequency discriminator," *IEEE Photon. Technol. Lett.*, vol. 18, no. 19, pp. 2062-2064, Oct. 2006.

[22] J. J. Dong, X. L. Zhang, J. Xu, D. X. Huang, S. N. Fu, and P. Shum, "Ultrawideband monocycle generation using cross-phase modulation in a semiconductor optical amplifier," *Opt. Lett.*, vol. 32, no. 10, pp. 1223-1225, May 15 2007.

[23] S. L. Pan and J. P. Yao, "Switchable UWB pulse generation using a phase modulator and a reconfigurable asymmetric Mach-Zehnder interferometer," *Opt. Lett.*, vol. 34, no. 2, pp. 160-162, Jan. 2009.

[24] Q. Wang, F. Zeng, S. Blais, and J. P. Yao, "Optical ultrawideband monocycle pulse generation based on cross-gain modulation in a semiconductor optical amplifier," *Opt. Lett.*, vol. 31, no. 21, pp. 3083-3085, Nov. 2006.

[25] Q. Wang and J. P. Yao, "Switchable optical UWB monocycle and doublet generation using a reconfigurable photonic microwave delay-line filter," *Opt. Express*, vol. 15, no. 22, pp. 14667-14672, Oct. 2007.

[26] H. Chen, M. Chen, C. Qiu, J. Zhang, and S. Xie, "UWB monocycle pulse generation by optical polarisation time delay method," *Electron. Lett.*, vol. 43, no. 9, pp. 542-543, Apr. 2007.

[27] J. Q. Li, K. Xu, S. N. Fu, J. Wu, J. T. Lin, M. Tang, and P. Shum, "Ultra-wideband pulse generation with flexible pulse shape and polarity control using a Sagnac-interferometer-based intensity modulator," *Opt. Express*, vol. 15, no. 26, pp. 18156-18161, Dec. 2007.

[28] J. Q. Li, S. N. Fu, K. Xu, J. Wu, J. T. Lin, M. Tang, and P. Shum, "Photonic ultrawideband monocycle pulse generation using a single electro-optic modulator," *Opt. Lett.*, vol. 33, no. 3, pp. 288-290, Feb. 2008.

[29] J. Wang, Q. Z. Sun, J. Q. Sun, and W. W. Zhang, "All-optical UWB pulse generation using sum-frequency generation in a PPLN waveguide," *Opt. Express*, vol. 17, no. 5, pp. 3521-3530, Mar. 2009.

[30] Q. Wang and J. P. Yao, "Multi-tap photonic microwave filters with arbitrary positive and negative coefficients using a polarization modulator and an optical polarizer," *IEEE Photon. Technol. Lett.*, vol. 20, no. 2, pp. 78-80, Jan. 2008.

[31] S. L. Pan and J. P. Yao, "Optical generation of polarity- and shape-switchable UWB pulses using an chirped intensity modulator and a first-order asymmetric Mach-Zehnder interferometer," *Opt. Lett.*, vol. 34, no. 9, pp.1312-1314, May 2009.

[32] S. S. Mo and A. D. Gelman, "On the power spectral density of UWB signals in IEEE 802.15.3a," *IEEE Conference on Wireless Communications and Networking*, WCNC 2004, vol. 2, pp. 999-1003, Mar 2004.

[33] M. Z. Win, "Spectral density of random UWB signals," *IEEE Commun. Lett.*, vol. 6, no. 12, pp. 526-528, Dec. 2002.

[34] J. Romme and L. Piazzo, "On the power spectral density of time hopping impulse radio," *IEEE Conference on Ultra Wideband Systems and Technologies*, 2002, pp. 241-244, May 2002.

[35] K. S Shanmugan, "Estimating the Power Spectral Density of Ultra Wideband Signals," *IEEE International Conference on Personal Wireless Communications*, 2002, pp. 124-128, Dec. 2002.

[36] Y. P. Nakache and A. F. Molisch, "Spectral shape of UWB signals - influence of modulation format, multiple access scheme and pulse shape," *IEEE Vehicular Technology Conference 2003*, VTC 2003-Spring, vol. 4, pp. 2510 - 2514, Apr. 2003.

[37] P. Prommasuksakul, P. Supanakoon, S. Promwong, and J. Takada, "Power spectral density analysis of ultra wideband signal using pulse shape modulation," *Electrical Engineering/Electronics, Computer, Telecommunications and Information Technology International Conference* (ECTI-CON 2007), pp. 880-883, May 2007

[38] Di Benedetto and G. Giancola, *Understanding Ultra Wideband Radio Fundamentals*. *Upper Saddle River*. NJ: Prentice Hall, 2004.

[39] G. P. Agrawal, *Nonlinear Fiber Optics*. San Diego, CA: Academic, 2001.

[40] U. Gliese, S. Norskov, and T. N. Nielsen, "Chromatic dispersion in fiber-optic microwave and millimeter-wave links," *IEEE Trans. Microw. Theory Tech.*, vol. 44, no. 10, pp. 1716-1724, Oct. 1996.

Shilong Pan (S'06-M'09)received his B.S. and Ph.D. degrees in Electronics Engineering from Tsinghua University, Beijing, China, in 2004 and 2008, respectively.

In August 2008, he joined the Microwave Photonics Research Laboratory, School of information Technology and Engineering, University of Ottawa, Ottawa, ON, Canada, as a Postdoctoral Research Fellow. His current research interests are focused on microwave photonics, which includes photonic generation of microwave, mm-wave and THz based on fiber lasers and optoelectronic oscillators, UWB over fiber, and photonic microwave frequency measurement.

Dr. Pan is a member of OSA and IEEE/LEOS.

Jianping Yao (M'99-SM'01) received his PhD degree in Electrical Engineering in 1997 from the Universit de Toulon, Toulon, France.

He joined the School of Information Technology and Engineering, University of Ottawa, Ontario, Canada, in 2001, where he is currently a Professor, Director of the Microwave Photonics Research Laboratory, and Director of the Ottawa-Carleton Institute for Electrical and Computer Engineering. From 1999 to 2001, he held a faculty position with the School of Electrical and Electronic Engineering, Nanyang Technological University, Singapore. He holds a Yongqian Endowed Visiting Chair Professorship with Zhejiang University, China. He spent three months as an invited professor in the Institut National Polytechnique de Grenoble, France, in 2005.

His research has focused on microwave photonics, which includes all-optical microwave signal processing, photonic generation of microwave, mm-wave and THz, radio over fiber, UWB over fiber, fiber Bragg gratings for microwave photonics applications, and optically controlled phased array antenna. His research interests also include fiber lasers, fiber-optic sensors and bio-photonics. He is an Associate Editor of the International Journal of Microwave and Optical Technology. He is on the Editorial Board of IEEE Transactions on Microwave Theory and Techniques. Dr. Yao received the 2005 International Creative Research Award of the University of Ottawa. He was the recipient of the 2007 George S. Glinski Award for Excellence in Research. He was named University Research Chair in Microwave Photonics in 2007. He was a recipient of an NSERC Discovery Accelerator Supplements award in 2008. Dr. Yao has authored or co-authored over 150 papers in refereed journals and over 120 papers in conference proceeding.

Dr. Yao is a registered professional engineer of Ontario. He is a fellow of the Optical Society of America and a senior member of IEEE Photonics Society and IEEE Microwave Theory and Techniques Society.